Hindawi
Geofluids
Volume 2022, Article ID 6026316, 18 pages
https://doi.org/10.1155/2022/6026316

Research Article

Analysis of Seismic Damage Modes of Landslides Containing Tunnels under Horizontal Earthquake Action

Hao Sun,[1,2] **Honggang Wu**,[2] **Zhigang Ma**,[1,2] **Zhou Yuan**,[1,2] **and Kang Feng**[1,2]

[1]*Southwest University of Science and Technology of Civil Engineering and Architecture, Mianyang 621000, China*
[2]*Northwest Railway Academy Co., Ltd. of CREC, Gansu 730000, China*

Correspondence should be addressed to Honggang Wu; 271462550@qq.com

Received 3 October 2022; Revised 27 October 2022; Accepted 2 November 2022; Published 14 November 2022

Academic Editor: Yu Wang

With the vigorous development of railway and highway construction, tunnel construction often follows the mountains and rivers, crossing high-intensity landslide areas, and potential earthquakes triggering damage in areas including tunnel landslides have become a hot issue today. Based on this, this paper performs a shaker test on the tunnel-containing landslide body, inputs horizontal seismic waves, and tests the acceleration response data of different bits in the landslide body. By analyzing the temporal and frequency domain transformations of the acceleration response at different positions in the slope body combined with the deformation characteristics of the slope, and then analyzing the seismic response of the slope under the action of the front and back seismic sequences, the results show that (1) the existence of the tunnel has the effect of energy dissipation and vibration reduction, making the energy input at T8, and the measuring point on the upper part of the tunnel at the lowest. (2) When the seismic wave is transmitted, it will cause reflection around the tunnel, forming complex seismic wave field, resulting in the irregular distribution of acceleration amplification coefficient. (3) There is a high correlation between seismic responses of different levels. When the acceleration response of the preseismic response to the landslide-containing tunnel is not considered, the acceleration response of the postseismic response to the slope and the structure will be lower than the real value. (4) The sequence of failure at different locations of landslide mass containing tunnel is found through marginal spectrum analysis. It is concluded that the failure mode of landslide mass with tunnel is extrusion and sliding out of the middle slope. The research results can provide some reference for the reinforcement design of landslide with tunnel in high-intensity area.

1. Introduction

In recent years, with the rapid development of highway and high-speed railway construction in mountainous areas of China, tunnel construction from east to west and from plain to mountainous areas has become an inevitable trend. Under the action of a series of geological actions such as earthquake and other disturbance loads, the slope with no obvious deformation or relatively stable will also appear large deformation and even develop into landslide, forming "landslide tunnel," which will damage the existing tunnel to varying degrees and affect and even interrupt the normal operation of the tunnel [1–4]. Tunnel-landslide problem has become a hot issue in engineering construction. For this reason, we have counted some typical tunnel-landslide engineering cases, as shown in Table 1.

At present, many scholars have carried out extensive and in-depth research on tunnel-landslide system. Wu et al. [5, 6] have studied the oblique and parallel system of tunnel landslide and provided a certain basis for the construction and design of tunnel crossing landslide through the analysis of displacement, deformation, and strain. Many scholars have discussed the tunnel orthogonal system through large-scale geological model tests and summarized the stress mode and deformation characteristics of the tunnel orthogonal system [7, 8]. But these studies have focused on statics.

With the continuous development of tunnel crossing landslide engineering, the projects of tunnel crossing high-

Table 1: Typical engineering cases of tunnel crossing landslide under potential earthquake action.

Serial number	Tunnel's name	Slope structure	System type	Disaster type	Remarks
1	Sunjiayai tunnel	Along dipping-layered slope structure	Orthogonal-through the slide	Tunnel excavation construction, continuous rain	Chongqing-Wufeng expressway
2	Zhongzhai tunnel	Along dipping-layered slope structure	Orthogonal-through the slide	Tunnel excavation construction, continuous rain	Linshuang highway
3	Songpan tunnel	Loose broken body slope structure	Skew-down slip body	High-intensity seismic action	Chenglan railway
4	Guojia tunnel	Slope structure with soft top and hard base bottom	Orthogonal system-underpass slip body	High-intensity seismic action	Baoji-Lanzhou high-speed railway

intensity area are increasing year by year. Therefore, many scholars have carried out relevant research on tunnel landslide under earthquake action. Pai and Wu [9] carried out shaking table test for the first time, taking orthogonal tunnel underpass landslide as a typical case. The dynamic response of underpass tunnel lining structure was studied, which provided reference for tunnel construction in high-intensity area. He et al. [10] used MPM numerical implementation to better understand the cause and impact of 2008 Wenchuan earthquake on Daguangbao landslide and proposed a safety analysis method based on Bayesian network. Konagai et al. [11] analyzed and summarized Kizawa tunnel in Mid-Niigata earthquake, summarized the causes of tunnel damage, and put forward suggestions for tunnel repair. Lu and Hwang [12] studied the collapse mechanism of Dakai subway during the Kobe earthquake by using FLAC2D dynamic time-history analysis and modified cross-section deformation (MCSRD) method and analyzed the damage evolution process of subway tunnel, showing that inertia force has a great influence on seismic characteristics. Zhang et al. [13] summarized the cases of tunnel failure and discussed the damage classification in order to explore the possible causes of damage, such as seismic parameters, structural forms, and geological conditions, providing reference for improving the seismic design of tunnels. Wen et al. [14] studied the dynamic response of segment lining structure of mountain tunnel crossing fault and proposed that the influence range of tunnel structure and the setting method of segment lining structure could provide reference for tunnel design crossing fault.

Most of the above studies focus on the dynamic response of tunnel lining or discuss the failure mode of landslide alone. At present, there are few studies on the dynamic of landslide-containing tunnel. Therefore, it is necessary to develop the dynamic response mechanism of landslide with tunnel, so as to provide reference for the reinforcement design of landslide with tunnel.

In this paper, through shaking table test of tunnel landslide, the acceleration response data of landslide at each location under different intensity earthquake is obtained. The failure of earthquake and slope acceleration time history curve is analyzed jointly, and the dynamic transmission characteristics and failure mode of tunnel landslide under dynamic action are understood. By means of Fourier transform and correlation analysis, the correlation between the seismic action sequence of the first order and the seismic action of the second order is discussed, which provides a reference for the reinforcement of landslide-containing tunnel. The peak marginal spectrum amplitude and characteristic frequency of each landslide location were extracted by the Hilbert-Huang transform (HHT) to reveal the disaster mode with sliding tunnel.

2. Design of Shaking Table Model Test

2.1. The Experiment Purpose. As the main traffic lines in China pass through the complex and dangerous mountainous areas, more and more tunnels are built in the high-intensity areas in the west of China, often facing the problem of tunnel penetration landslide. The tunnel deformation in the slope area caused by the potential earthquake has become one of the major hidden dangers facing the operation and maintenance of the traffic tunnels in this area [15]. But based on the research so far, most of the seismic studies on landslide-containing tunnels focus on the dynamic response of tunnel lining structures. For example, Pai and Wu [9] studied the dynamic response of tunnel lining under landslide by shaking table test and revealed the characteristics of circumferential spatial dynamic response of tunnel lining structure; in Sun et al. [16], interaction analysis of equal pass pair bias tunnel-loess slope coupling system, the dynamic response, and failure mode of the loess slope bias tunnel are revealed. Of course, many scholars have also investigated the dynamic response of the landslide-containing tunnels. Jiang et al. [17] explored the dynamic response of tunnel slope with multiple arches under the excitation of different seismic waves with multiple inputs, and the acceleration distribution of slope with multiple arches under different seismic waves is revealed. Zhang et al. [18] explored the influence of the existence and location of tunnels on the dynamic response of slope through numerical simulation and shaking table study.

Due to the complexity of seismic-tunnel-landslide terrain conditions, at present, the research remains on the dynamic response of tunnel lining structure and slope. The weak position and disaster mode of landslide-containing tunnel have not been given clear guidance. To effectively protect the tunnel structure and landslide safety protection, it is necessary to understand the weak link of seismic landslide with tunnel and reveal its motion law. Therefore, this paper is aimed at revealing the acceleration distribution law of landslide-containing tunnel, analyzing the seismic

(a) (b)

Figure 1: Shaker overview diagram. (a) Shaker system diagram. (b) Boundary processing diagram.

weak position of landslide-containing tunnel, and exploring the motion law of each position of the landslide under earthquake action, and the catastrophe model of landslide-containing tunnel under earthquake action is proposed. It is expected to provide reference for engineering construction and reinforcement of tunnel landslide.

2.2. Model Similarity Design and Model Boundary Processing. In order to simulate the dynamic characteristics of the slope with tunnel, we used shaking table to load the seismic wave to observe the dynamic response in the slope and bedrock (Shaker system as shown in Figure 1(a)). In shaking table model tests of engineering structures, it is quite difficult to completely satisfy the model similarity, but the main influencing factors can generally be satisfied. However, in the shaking table model test involving soil medium, due to the limitation of the bearing capacity of the shaking table, it is not easy to satisfy the similarity relation of the full mass model with additional counterweight. In addition, considering the similarity of material constitutive properties, the incomplete mass model with the similarity ratio of mass density 1 : 1 is often adopted in shaking table test. Therefore, the test adopts the loose similarity between the model system and the prototype system, and the gravity distortion is allowed [19]. On the basis of determining the basic parameters of basic length $(C_l = 1/100)$, mass density $(C_\rho = 1)$, and elastic modulus $(C_E = 1/100)$, similarity ratios of other physical quantities are derived based on Buckingham π theorem [20]. According to the similitude relationship of the physical conditions, geometric conditions, dynamic equilibrium conditions, etc., the similitude relationships are expressed as Equations (1)–(6) [21]. The specific similarity ratio parameters are shown in Table 2.

$$C_\sigma = C_E C_\varepsilon, \tag{1}$$

$$C_\varepsilon = C_l C_\rho C_E^{-1}, \tag{2}$$

$$C_c = C_E C_\varepsilon, \tag{3}$$

$$C_a = C_l C_t^{-2}, \tag{4}$$

$$C_v = C_l C_t^{-1}, \tag{5}$$

Table 2: Test similarity ratio.

Physical quantities	Similar relationship	Design similarity ratio
Length (l)	C_l	1/100
Elastic modulus (E)	C_E	1/100
Density (ρ)	C_ρ	1
Time (t)	$C_t = C_L^{1/2}$	1/10
Poisson's ratio (μ)	C_μ	1
Stress (σ)	$C_\sigma = C_E C_\varepsilon$	1/100
Strain (ε)	$C_\varepsilon = C_l C_\rho C_E^{-1}$	1
Cohesion (c)	$C_c = C_E C_\varepsilon$	1/100
Internal friction angle (φ)	C_φ	1
Acceleration (a)	$C_a = C_l C_t^{-2}$	1
Speed (v)	$C_v = C_l C_t^{-1}$	1/10
Frequency (f)	$C_f = C_t^{-1}$	1/0.1

$$C_f = C_t^{-1}, \tag{6}$$

where $C_\mu = C_\varphi = 1$, t is time, μ is Poisson's ratio, σ is stress, ε is strain, c is cohesion, φ is angle of internal friction, a is acceleration, v is velocity, and f is frequency.

Considering the influence of "rigid model box boundary effect," the model box boundary needs to be processed [22, 23]. In order to reduce the influence of boundary effect in the direction perpendicular to horizontal vibration inside the model box, 20 mm thick XPS extruded plate with compressive strength of 250 kPa and density of 35 kg/m^3 is adopted. This kind of foam plastic plate has the best compressive performance. XPS extruded plate is always in a linear elastic state during the test loading process. The dynamic elastic modulus of XPS extruded plate is 7~9 MPa. A smooth PVC film was pasted along the horizontal vibration direction to reduce the friction between the side wall of the model box and the soil. A layer of XPS extruded plate is laid on the two sides parallel to the tunnel to reduce the reflection of waves on the boundary surface. Seismic waves are input from the

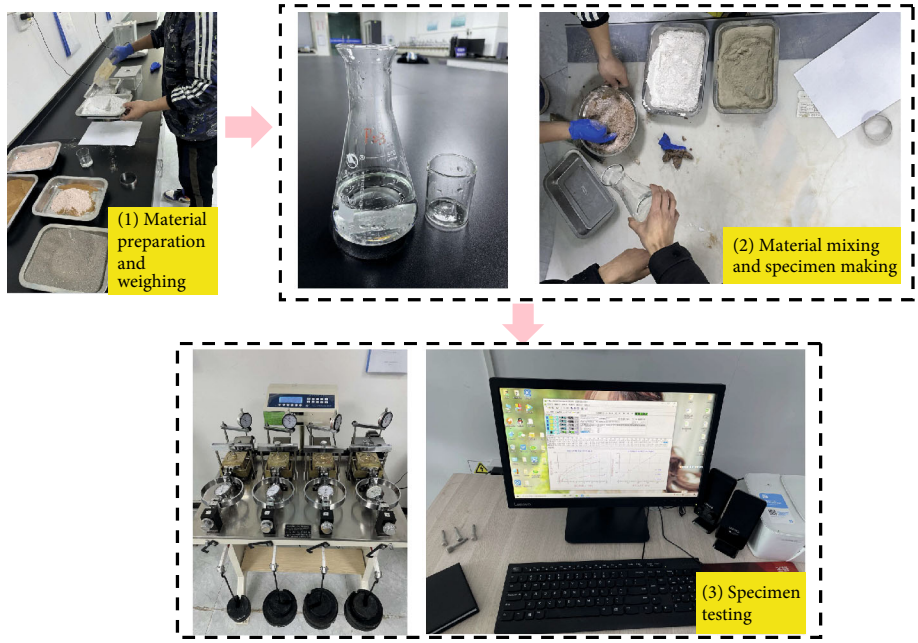

Figure 2: Model similar materials and sample tests.

Table 3: Model similarity parameters.

Material	Quartz sand (g)	Red clay (g)	Barite powder (g)	Gypsum powder (g)	Talcum powder (g)	Water (g)	Bulk density γ (kN m^{-3})	Elastic modulus E (GPa)	Cohesion c (kPa)	Internal friction angle φ (°)	Tensile strength σ_t (MPa)	The compressive strength σ_c (MPa)
The surrounding rock	16	6	24	1	/	2	15.65	0.03	25.07	39.32	/	0.12
The sliding body	70	/	/	3	/	2	13.77	/	17.94	38.10	/	/
Sliding zone	4	6	/	/	7	4	12.51	/	5.68	39.81	/	/
The lining				1.1		1		0.77	/	/	0.05	0.58

bottom of the model box, so there should be no relative sliding between the filling material and the bottom plate of the model box. In order to ensure good bonding between them, a layer of gravel soil 5 cm thick is laid on the bottom plate of the model box to increase the friction force, and the particle size of gravel is about 1 cm [14]. The bottom plate is treated as friction boundary to limit and reduce the relative displacement between the bottom and the soil. The boundary processing diagram of shaking table model is shown in Figure 1(b).

2.3. Test Similar Material Selection and Model Making. In shaking table model test, the key to success lies in the preparation of similar materials. The selection of similar raw materials is also the first consideration in the preparation of similar materials for rock mass. The mechanical properties of different rock strata can be changed by selecting different materials or changing their proportions. In order to ensure that the slope similar materials prepared can meet the needs of the test, the following principles are considered in the selection of similar materials: (1) in the selection of raw materials for similar materials, it is necessary to ensure that the similarity of mechanical properties between the similar materials and the prototype is higher, so that it can better simulate the rock structure. (2) The physical and mechanical parameters of samples prepared by one or several similar materials have a large adjustable range. Changing the ratio of one or several materials can change the mechanical parameters of the samples. (3) Similar materials used as casting models can still maintain good stability when temperature, time, and other factors change. (4) The raw materials used in the experiment come from a wide range of sources and are cheap. (5) Raw materials are harmless to human body and do not damage human health.

The raw materials selected for this test are quartz sand, red clay, gypsum, talc, barite powder, water, and so on. Quartz sand in similar raw materials can not only play the role of skeleton support but also increase the internal friction angle and bulk density of similar materials. Barite powder is mainly used to increase the counterweight of model

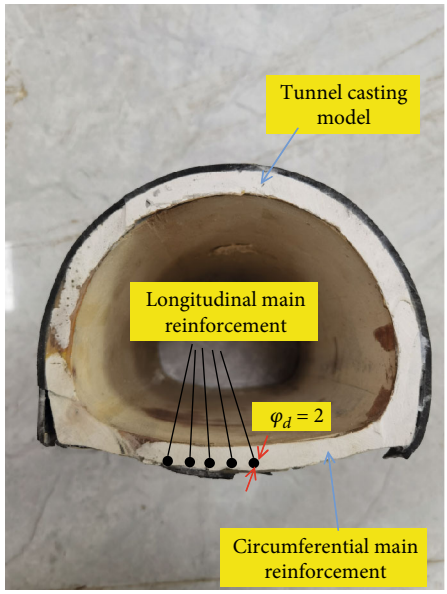

Figure 3: Tunnel model.

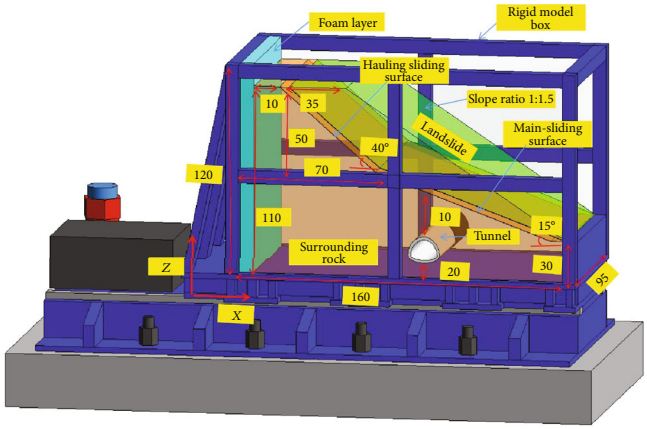

Figure 4: Design drawing of shaking table test model (cm).

materials. Talc, gypsum, and red clay are used as auxiliary adjusting materials to adjust the density, elastic modulus, and compressive strength of similar materials. Water can be used to regulate the cohesion of the material and control the moisture content. The specific preparation of similar material parameters is shown in Figure 2, and the obtained similar model parameters are shown in Table 3.

According to geometric similarity, the maximum span of the lining model is 19.3 cm, the height is 14.6 cm, and the thickness is 0.6 cm. Tunnel lining is mainly formed by mixing gypsum powder and water in a certain proportion, and the proportion parameters are shown in Table 3. The effectiveness of using gypsum as a similar material to simulate C30 concrete has been confirmed in previous studies [24]. A 0.2 mm diameter steel wire mesh is used to approximate the annular main reinforcement and distributed reinforcement in the lining structure. The tunnel model is shown in Figure 3.

Before the model test, we designed the experiment in advance. The height of the model is 110 cm, the width is 95 cm, the length is 160 cm, the slope of the front edge of the overlying sliding body is 15°, the slope of the back edge is 40°, the slope ratio of the whole sliding body is 1 : 1.5, and the tunnel is in the middle of the main sliding section of the landslide, 10 cm away from the sliding zone and 20 cm away from the bottom of the model. The model was composed of three kinds of soil materials: the lower bedrock, the middle slide zone, and the overlying slide body. The model design is shown in Figure 4. We focus on the dynamic response of landslide with tunnel under seismic action, so the slip surface is set up in advance during model design. In order to make the sliding process continuous, according to the requirements of physical model test, referring to relevant specifications [25, 26] and combined with the actual guiding parameters of relevant engineering, the appropriate proportion of similar materials in the sliding zone was determined through indoor sample test, mainly meeting the similarity of c and φ. The sliding-band similar materials are simulated to meet the requirements, and the cohesion and internal friction angle are similar. The initial slip surface of slope is simulated by using similar materials of slip zone, and the effectiveness of this method to simulate the slip surface has also been confirmed in previous studies [27].

When the shaking table test model was prepared, materials were first mixed according to the similar material ratio, and then, the model materials were placed layer by layer, each layer was 10 cm thick and tamped layer by layer. As the model is filled, the tunnel structure is installed at the target position. The specific filling process is shown in Figure 5. The full view of the model is shown in Figure 6.

2.4. Experimental Loading Scheme and Sensor Layout. EL Centro wave was used in this experiment, which was the first seismic wave with the maximum acceleration over 300 gal captured in the United States in 1940 [28]. The loading direction was loaded along the horizontal direction, and the waveform used was the same each time during the loading process, except that the peak acceleration increased. We carried out three loads: case 1: 0.1 g low-intensity seismic wave, case 2: 0.2 g medium-intensity seismic wave, and case 3: 0.4 g high-intensity seismic wave. The design of loading conditions is shown in Figure 7.

Since the experiment focuses on studying the acceleration transfer characteristics of landslide with tunnel, acceleration sensors are mainly used to monitor the dynamic characteristics of slope during loading. Five sensors are arranged in the slope body at the interface between landslide and sliding surface, numbered T20, T21, T15, T16, and T8 from top to bottom. Three sensors are arranged on the mountain side of the tunnel (axis 1-1), numbered T7, T5, and T4, respectively, from top to bottom. Three sensors, numbered T2, T13, and T6, were placed above and below the tunnel vault. Three sensors, numbered T8, T6, and T1 from top to bottom, are arranged on the river side of the tunnel. The layout of measuring points is shown in Figure 8.

Figure 5: Shaking table model filling process.

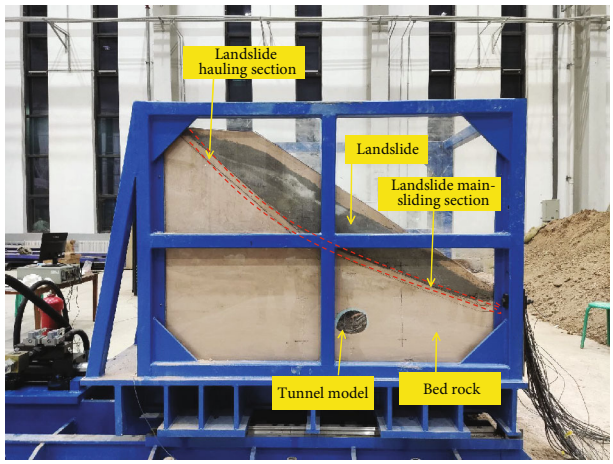

Figure 6: Overall view of the model.

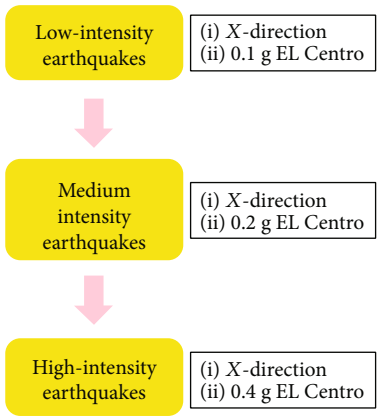

Figure 7: Design of loading conditions.

3. Experimental Results and Analysis

3.1. Analysis of Acceleration Time-History Curve of Landslide Deformation and Slide Zone Position. In order to study the dynamic response of the landslide under the earthquake, the acceleration response time-history curves of different positions of the slide surface inside the slope were extracted and analyzed in combination with the failure of the landslide. Figure 9 shows the slope failure and acceleration time-history curve under the action of low-intensity earthquake (0.1 g), medium-intensity earthquake (0.2 g), and high-intensity earthquake (0.4 g).

It can be seen from Figure 9(a) that, under the action of low-intensity earthquake, the accelerated response at T15 and T21 on the slope reached the peak first and was more intense than other positions and reached the peak later at the top of the slope, the middle, and lower parts of the broken rock and the foot of the slope. Combined with the deformation analysis of the slope body, the small cracks appear in the middle of the landslide under the action of seismic waves in the process of upward transmission. Partial spalling occurred at the top of the slope, and smiling tensile cracks occurred at the top and left and right sides. Local spalling occurred at the foot of the slope.

With the further loading, under the action of moderate earthquake, the peak acceleration of each position of the slide zone almost reached the maximum at the same time, and the peak acceleration of T16 position in the middle and lower part of the landslide was the minimum, while the peak acceleration of the middle and upper part of the landslide was almost the same degree of intensity. Under the action of earthquake, the damage of slope body shows that the cracks of the upper slope body continue to expand, the cracks of the top extend to the slope body, and the cracks on the left and right sides extend to the sliding zone from top to bottom. The slope surface gradually loosens under the earthquake action and produces further spalling. Spalling

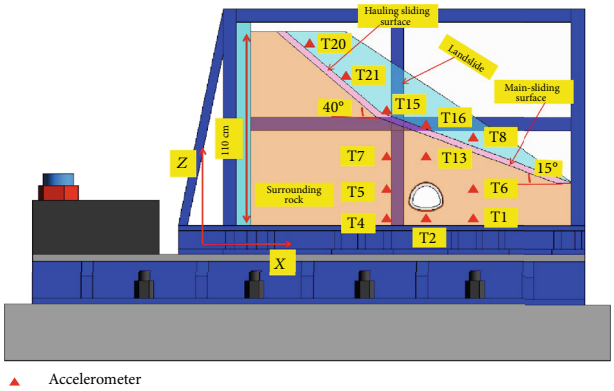

Figure 8: Layout of measuring points.

at the foot of the slope is further enhanced, and a few accumulations are formed at the bottom of the slope.

Under the action of high-intensity earthquake, the acceleration at each position of the landslide body reaches the maximum value almost at the same time, the dynamic response of the landslide body is more obvious, and the destruction phenomenon at each position of the landslide is more intense. The fracture depth of the upper slope gradually increased and formed a "U" shaped groove on the upper slope. The left and right sides of the slope extend from the top of the slope through the slide zone to the middle of the landslide, deep into the lower bedrock, and the length of the fracture increases gradually. The spalling surface of the slope extends from the foot of the slope to the central slope. The exfoliation blocks from the upper and lower parts of the slope form a large amount of accumulation at the toe of the slope.

Combined with the acceleration time-history curves of the measuring points of the slope and inside the slope, it can be seen that under the action of different seismic intensities, the peak acceleration of the measuring point T16 at the top of the tunnel is always the minimum. This may be because the existence of the tunnel makes the location be buffered to a certain extent, so the earthquake damage at this location is always minimal. This indicates that the existence of tunnel has a certain damping effect on the slope. It can be seen from the failure phenomenon of the upper slope and the middle slope that there are large cracks and spalling slots in these positions. Meanwhile, it can be found from the acceleration time-history curve that the response to these positions is the most obvious, indicating that the upper slope and the middle slope may be the weakest positions in the whole slope, which provides a certain basis for the reinforcement of tunnel landslide.

3.2. Analysis of Time-History Curve of Acceleration in Slope Bedrock. According to the above experimental phenomena and the analysis of the acceleration time-history curve arranged along the slip zone, it can be seen that after the earthquake of different intensities, the tensile cracks gradually penetrate down into the surrounding rock along the position of the slip zone and the slide body, making the whole slope appear a downward sliding trend. Therefore, in order to explore the dynamic response of different positions in the surrounding rock, measurement points at different positions were selected for analysis. Here, we specify axes 1-1 (T4, T5, and T7), 2-2 (T2, T13, and T16), and 3-3 (T1, T6, and T8) from inside the slope to outside. The time-peak acceleration curves of the above axis positions were selected for analysis.

Figure 10 shows the time-peak acceleration curves of different measuring points in bedrock under the action of earthquakes of different intensities. Figure 10(a) shows the time-peak acceleration curves of measuring points on different axes in bedrock under the action of low-intensity earthquake. It can be seen from the figure that under the excitation of low-intensity earthquake, the peak acceleration appears the regular distribution with elevation increase. However, there are great differences in peak time of each axis. The peak time of each measuring point at axis 1-1 is relatively close, while the peak time of each measuring point at axis 2-2 and axis 3-3 is quite different after crossing the tunnel. With the increase of earthquake intensity, combined with Figure 10(b), under the action of moderate earthquake, the peak time of each measuring point only fluctuates slightly, which indicates that the tunnel setup has obvious influence on the peak acceleration time, and the difference of peak acceleration time under the action of moderate earthquake is almost 0. In Figure 10(c), the time-peak acceleration curve appears similar to Figure 10(b), and this shows that the time difference between peak accelerations is nearly the same as the earthquake intensity increases.

Combined with the analysis of the location of each measuring point, it can be seen that in the case of horizontal low-intensity earthquake, seismic wave takes the lead to the position 1-1 on the axis. Due to the low earthquake intensity, the bedrock gives full play to its damping effect, resulting in a slight difference in the peak arrival time of each measuring point at the position 1-1 on the axis. As the horizontal seismic wave is transmitted to the position 2-2 of the axis, due to the existence of the tunnel, and the measuring point at T13 is close to the slip zone, the damping characteristics of this position are changed, and the damping performance at the lower T2 position is stronger, resulting in a large gap between the peak time at the upper and lower positions of the tunnel. When the horizontal seismic wave reaches position 3-3, T6 is located in the middle of the tunnel, and the tunnel gives full play to its damping effect as a structure, resulting in a late peak time at this position. However, with the increase of seismic intensity, the intensity has exceeded the damping threshold of bedrock and tunnel, resulting in the arrival time of peak acceleration at each location is basically the same.

3.3. Analysis of Acceleration Amplification Coefficients at Various Positions in the Landslide Body. In order to explore the characteristics of acceleration transfer in landslide with tunnel, we further processed the acceleration peaks at each position under various working conditions and defined the ratio of the peak acceleration at each position to the peak acceleration at T1 position at the bedrock bottom of slope toe as acceleration amplification coefficient (PGA

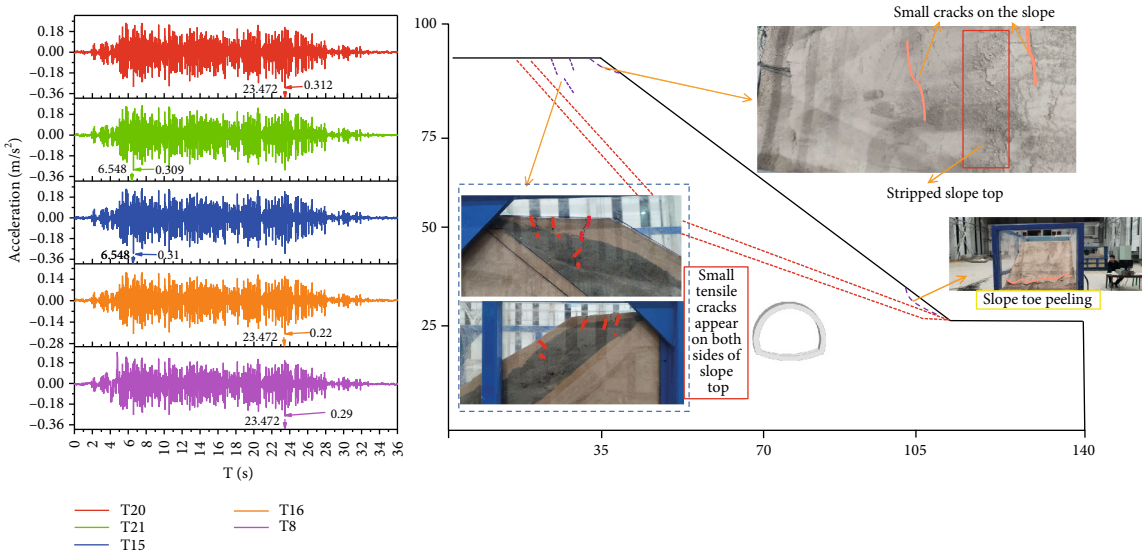

(a)

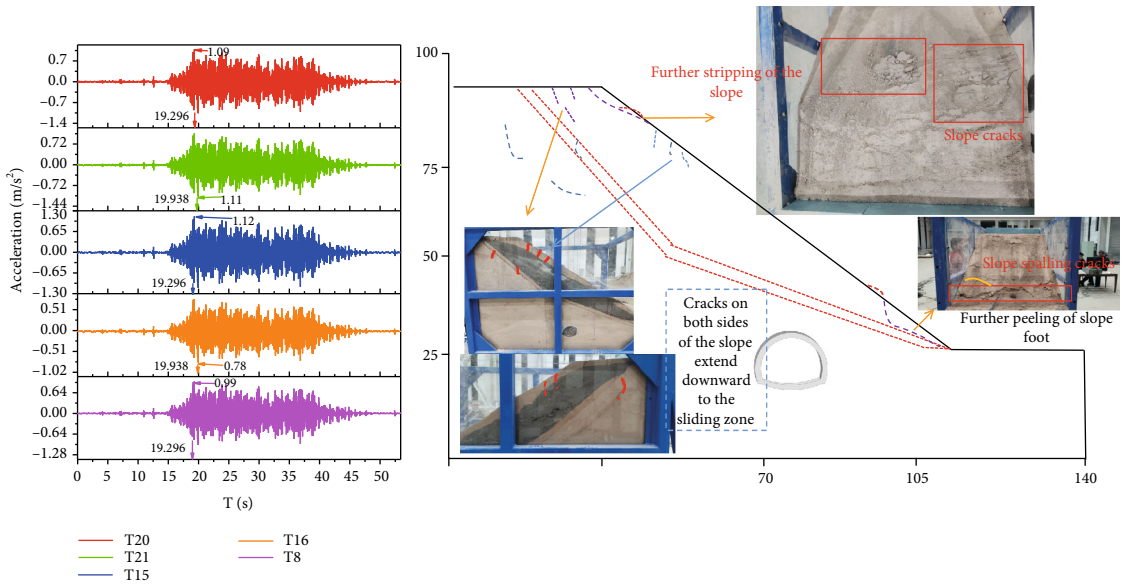

(b)

Figure 9: Continued.

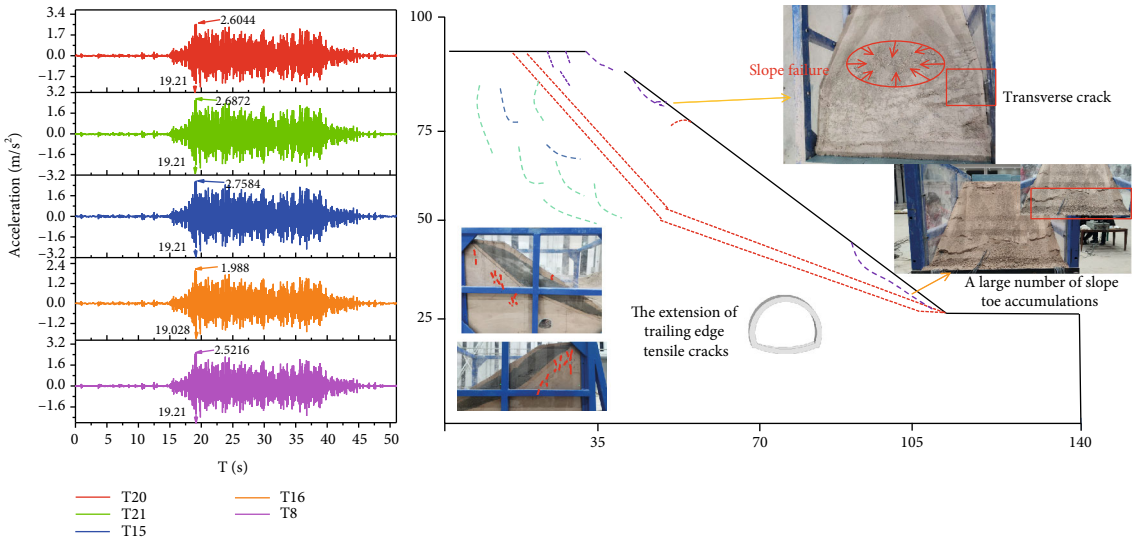

(c)

Figure 9: Time-history curves and deformation characteristics of slope in-plane acceleration under different earthquake intensities. (a) Acceleration time-history curve and deformation characteristics of slope under low-intensity earthquake. (b) Acceleration time-history curve and deformation characteristics of slope under moderate earthquake. (c) Acceleration time-history curve and deformation characteristics of slope under high-intensity earthquake.

amplification coefficient). The PGA amplification coefficients of internal axes 1-1, 2-2, and 3-3 and slope surface of bedrock were selected for analysis.

Figure 11 shows the acceleration amplification coefficients of each side point at different axis positions in the slope body. It can be seen from the figure that the acceleration amplification coefficients of each axis position show a relatively complex trend under the action of earthquakes of different intensities. It can be seen from Figure 11(a) that at axis 1-1, the acceleration amplification coefficients of each measuring point under the action of low-intensity earthquake and high-intensity earthquake show a trend of amplification, while under the action of medium-intensity earthquake, the acceleration amplification coefficients show a trend of first decrease and then increase. It can be seen from Figure 11(b) that the measuring points at the 2-2 position of the tunnel axis show a trend of first increasing and then decreasing under the action of earthquakes of different intensity. At the position of axis 3-3, the accelerated amplification coefficients of each measuring point show an increasing trend under the action of low-intensity earthquakes, while the accelerated amplification coefficients of each measuring point show an increasing trend first and then decreasing trend under the action of medium-intensity and high-intensity earthquakes. Combined with the analysis of the above phenomena, it can be seen that a complex seismic wave field will be formed under the coupling action of different input peak seismic waves and tunnels, and this wave field will have a complex influence on the acceleration transmission of surrounding soil, especially in the position of measuring points close to the tunnel.

Figure 12 shows the acceleration amplification coefficient of each measuring point at the interface between the slip body and the slip zone. As can be seen from the figure, under the earthquake of different intensities, the acceleration amplification coefficient does not increase with the increase of the height but decreases sharply at the position of 1/2 of the slope height first and then increases sharply. After the slope angle T15 position, the acceleration amplification coefficient shows a relatively gentle or even decreasing feature with the increase of the height. Combined with the position analysis of each measuring point, it can be seen that the reason for the rapid decrease is that the landslide has a strong suppression effect on the horizontal seismic wave under the coupling effect of seismic wave and tunnel. The acceleration amplification coefficient at the angle of T15 increases sharply. Compared with the acceleration amplification coefficient at the measured point above it, it indicates that the small topographic gap is likely to cause the surge of horizontal seismic acceleration at the interface between the slip zone and the slip body. This can also be effectively verified by the deformation characteristics of the landslide in Figure 9(c). After the earthquake, the tensile crack of the landslide extends to the corner position of the lower part of the slope. From the above analysis, it can be seen that in the landslide with tunnel under earthquake action, the corner position at the interface between the slide zone and the slide body is the weak link in the slope, and the effective suppression of vibration intensity at this position is the key to prevent landslide damage, which provides a reference for the reinforcement of the landslide with tunnel.

3.4. Correlation Analysis of Spectrum Amplitude Changes. In order to further explore the transfer characteristics of acceleration in tunnel landslides, the spectral amplitude feature points were extracted by Fourier transform, and the correlation of seismic acceleration responses was analyzed by

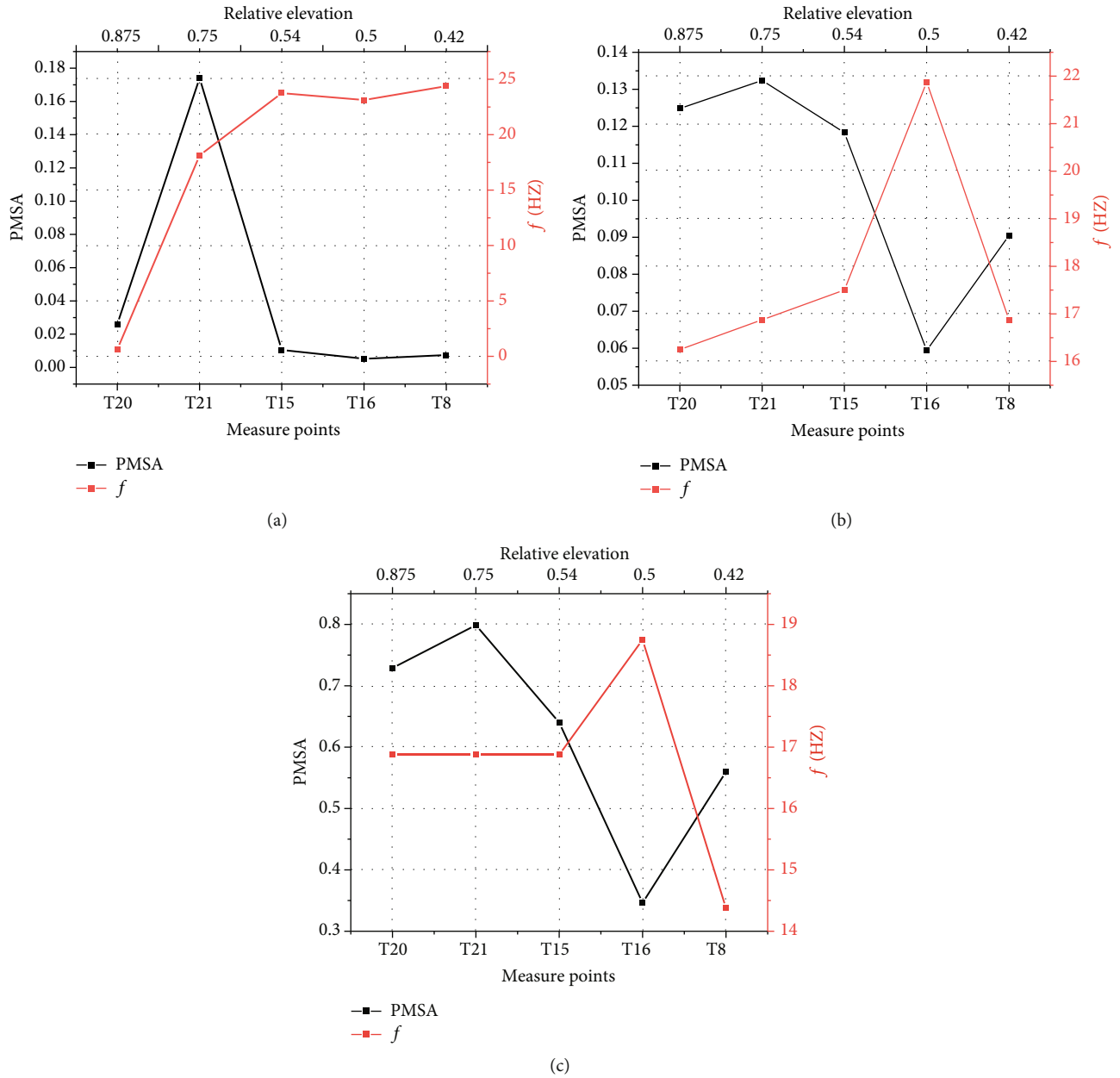

Figure 10: Time-peak acceleration curves of different measuring points in bedrock under different earthquake intensities. (a) Time-peak acceleration diagram of each measuring point in bedrock under the action of low-intensity earthquake. (b) Time-peak acceleration diagram of each measuring point in bedrock under the action of moderate earthquake. (c) Time-peak acceleration diagram of each measuring point in bedrock under high-intensity earthquake.

statistical principles. Figure 13 shows the amplitude scatter matrix of different measuring points in the slope.

According to the amplitude scatter matrix analysis of each measuring point at the interface between the sliding body and the sliding zone in Figure 13(a), it can be seen that there is a positive correlation between seismic responses at all levels, and the correlation coefficient is relatively high. The seismic response at the junction of the slide body and the slip belt was 0.1 g and 0.2 g, the correlation coefficient of 0.4 g was 0.98656 and 0.95499, and the correlation coefficient of 0.2 g and 0.4 g was 0.98557. Earthquakes of all magnitudes have a high correlation coefficient with foreshock, which indicates that the occurrence of foreshock directly affects the acceleration response of post-first-order earthquakes to landslides containing tunnels. The landslide failure process mentioned above can be verified. After the foreshock response, the second-order ground motion response has serious damage to the upper slope body when the vibration response occurs everywhere, and tensile cracks extend from top to bottom to the interior of bedrock.

As can be seen from Figure 13(b), the correlation coefficient between 0.1 g and 0.2 g ground motion responses at each axis inside the bedrock is 0.89066, and the correlation coefficient between 0.2 g and 0.4 g ground motion responses

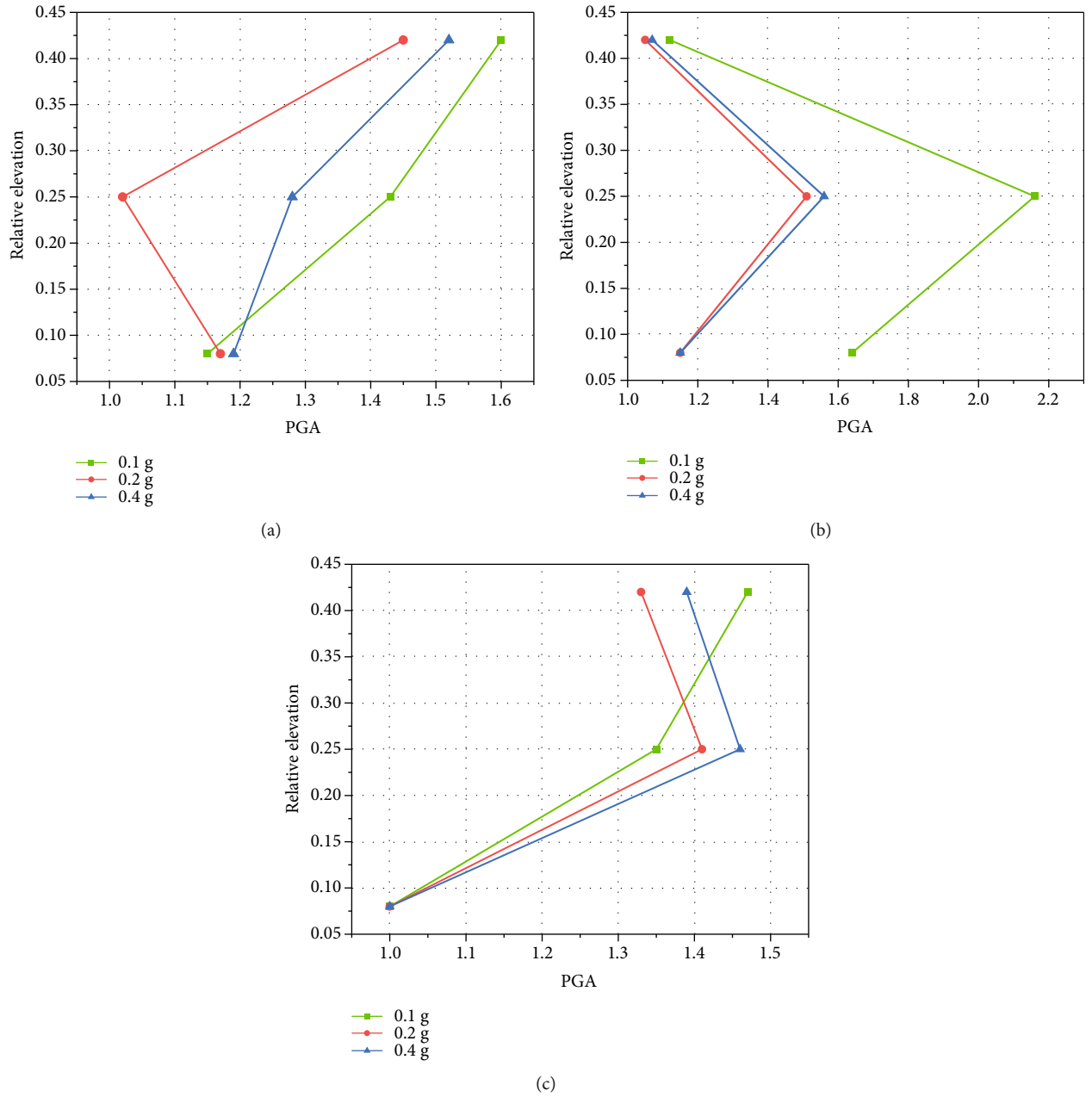

Figure 11: Acceleration amplification coefficients of axes in bedrock under earthquake of different intensities. (a) Acceleration amplification coefficient of axis 1-1 under different intensity earthquake action. (b) Axis 2-2 position acceleration amplification coefficient under different intensity earthquake action. (c) Acceleration amplification coefficient of axis 3-3 under different intensity earthquake action.

is 0.9533, indicating that there is a high correlation between adjacent seismic responses when earthquakes occur in the bedrock. The correlation coefficient between 0.1 g and 0.4 g ground motion responses is 0.7641, indicating that there is a significant correlation between the two ground motion responses. As can be seen from the landslide failure mentioned above, when the ground motion response is 0.1 g, only the upper slope body is damaged, and the lower bedrock is always in a relatively stable state. When the ground motion response reaches 0.4 g, tensile cracks appear in the middle and lower slope body, so the correlation coefficient between 0.1 g and 0.4 g of ground motion response decreases slightly.

The above analysis shows that the correlation coefficient between ground vibration responses is high in the failure process of the landslide-containing tunnel. If the acceleration response of the preseismic response to the landslide-containing tunnel is not considered, the acceleration response of the post-first-order seismic response to the slope and the structure will be lower than the real value.

4. Discussion

Through the above analysis, it is found that the slope with tunnel landslide shows very obvious variation characteristics

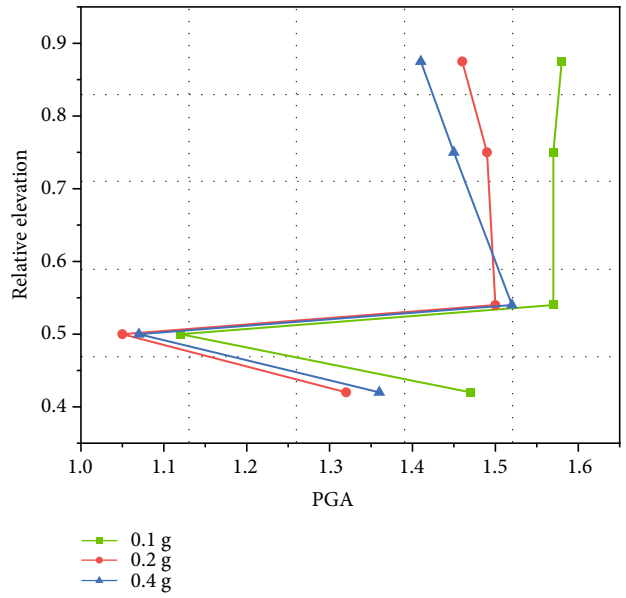

Figure 12: Acceleration amplification coefficient of the interface of the sliding body slide of the sliding body with.

to the earthquake. Combined with the previous studies [29] on the dynamic response of the slope without tunnels under the action of earthquakes, there is a large gap between the acceleration amplification coefficient curve of the slope surface in the previous research and the slope acceleration amplification coefficient curve presented in Section 3.3. In the past, the slope magnification factor for slopes without tunnels showed a gradually increasing trend with the elevation, while the slope acceleration magnification factor curve shown in Section 3.3 showed a significant decrease and then gradually increased with the elevation. Therefore, it can be foreseen that the existence of the tunnel may change the failure mode of the slope to a certain extent. In addition, some previous studies on failure modes of slopes without tunnels are summarized, as shown in Table 4. In order to further explore its change law, we select A20, A21, A15, A16, and A8 measuring points located inside the slope for HHT transformation [30–33], and the marginal spectrum of the above measuring points is extracted to analyze the energy variation characteristics in the frequency domain of the transmission process of seismic wave in the landslide surface.

4.1. HHT and Marginal Spectrum Theory. HHT transform is a random signal processing method proposed by Huang et al. [31]. Here, we briefly describe the HHT transformation. First, we need to perform empirical mode decomposition of the original signal, and after EMD decomposition, several order intrinsic mode functions (IMF) with frequency distribution from high to low can be obtained from a complex random time series; then, we perform Hilbert transformation on each IMF. Finally, the instantaneous frequency, Hilbert spectrum, and Hilbert marginal spectrum of each order of the original complex random time series are obtained. The acquisition process is as follows:

The initial processed acceleration data $X(t)$ is subjected to empirical mode decomposition (EMD) to obtain a series of intrinsic mode function (IMF) components of $X(t)$, denoted as $Y(t)$:

$$Y(t) = \frac{1}{\pi} P \int_{-\infty}^{+\infty} \frac{X\left(t'\right)}{t - t'} dt'. \tag{7}$$

The obtained $Y(t)$ is used to construct the analytical signal, which is recorded as $Z(t)$, and the analytical equation is derived to obtain the instantaneous frequency spectrum curve of IMF. The process is as follows:

$$Z(t) = X(t) + iY(t) = a(t)e^{i\theta(t)}, \tag{8}$$

where $a(t) = [X^2(t) + Y^2(t)]^{1/2}$ is the instantaneous amplitude, $\theta(t) = \arctan[Y(T)/X(t)]$ is the instantaneous phase, and instantaneous frequency is $\omega(t) = d\theta(t)/dt$; then, we can derive

$$Z(t) = \sum_{j=1}^{n} a_j\left(t, \omega_j\right) e^{i\int \omega_j(t)dt}. \tag{9}$$

The Hilbert spectrum $H(t, \omega)$ can be obtained by combining all IMF amplitudes decomposed by $X(t)$ in the time-frequency domain.

$$H(t, \omega) = \sum_{1}^{n} a_j(t, \omega). \tag{10}$$

Equation (11) characterizes the distribution of signal energy in the time-energy-frequency three-dimensional space defined as Hilbert spectrum $H(t, \omega)$. Integrating Hilbert spectrum on the timeline yields a marginal spectrum $h(t, \omega)$:

$$h(t, \omega) = \int_{0}^{T} H(t, \omega)dt. \tag{11}$$

When the seismic wave is transmitted in the landslide (slope), if there is earthquake damage in a certain part, then the energy cannot be transmitted completely there, and the loss of energy will cause the sharp fluctuation and mutation of the marginal spectrum [33]. Based on this, we analyze the marginal spectrum of landslide with tunnel.

4.2. Marginal Spectrum Analysis of Each Measuring Point near the Sliding Surface under Different Earthquakes. Figure 14 shows the marginal spectrum curve of the measuring points near the landslide surface with tunnel. As can be seen from the figure, the marginal spectrum curve of landslide sliding surface under the action of low-intensity earthquake is obviously different from that under the action of medium-intensity and high-intensity earthquake. Under the action of low-intensity earthquake, the marginal spectral peak at T21 in the middle of the slope is obviously stronger than that at other locations, and the marginal spectral peaks

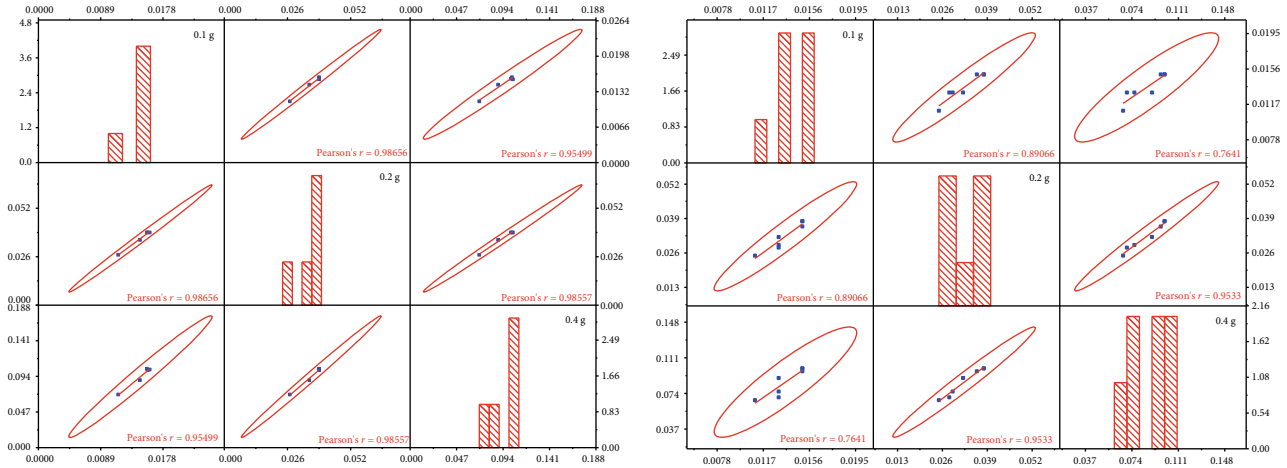

Figure 13: Amplitude scatter matrix. (a) Amplitude scatter matrix of measuring points on interface between slip zone and slip body. (b) Amplitude scatter matrix of each measuring point in bedrock.

Table 4: Failure mode of slope without tunnel.

Author	The types of slope body	Failure mode
Yu [34]	Loess slope with structural joints	Push on failure The collapse of destruction
Yang [35]	Foundation and overlay slope	Overall pull fracture of slope top-shear failure of slope foot Slope foot collapse-internal fracture of soil-sliding failure of sliding body Trailing edge tension-soil internal fracture-slope shear failure
Wang [36]	Gravel soil slopes and clay slopes	Push type failure

of T20, T21, and T15 near the slope sliding surface from top to bottom are close under the action of medium- and high-intensity earthquakes. It is worth noting that with the increase of earthquake intensity, the marginal spectrum peak at each position increases in different intensities; however, at T21 in the middle of the slope, abnormal characteristics appear during the action of low-intensity earthquake and medium-intensity earthquake, and the marginal spectral peak at this location under the action of low-intensity earthquake is greater than that under the action of medium-intensity earthquake. This indicates that the middle part of the slope may be the most sensitive part of the landslide mass containing tunnel, and under the action of low-intensity earthquake, the seismic damage may reach a certain damage intensity, so that the damage at this location will not be enhanced under the action of slightly strong earthquake. At the same time, the peak value of marginal spectrum at T16 at the top of the tunnel is the smallest under the action of earthquakes of all intensities. This shows that the seismic damage suffered by this location during earthquake is the smallest, and the existence of the tunnel has a certain damping effect on the surface of the above slope. This corroborates with the content of Section 3.

4.3. Analysis of Energy Variation Characteristics of Marginal Spectrum in Frequency Domain under Different Intensity Earthquakes. In order to further reveal the above contents, we extracted and analyzed the marginal spectral peak (PMSA) and characteristic frequency (f) of each measuring point near the sliding surface of the slope. Based on the research of previous scholars [32], the energy variation characteristics in frequency domain of seismic wave transmission process at each position of sliding surface of landslide mass with tunnel under horizontal earthquake are explored.

Figure 15 shows the marginal spectral peak and characteristic frequency curve of each measuring point under the action of earthquakes with different intensities. According to the analysis in Figure 15(a), under the action of low-intensity earthquake, the marginal spectral peaks and characteristic frequencies at T8, T16, and T15 in the downhill are basically stable with the increase of relative elevation. It shows that these locations were not damaged by low-intensity earthquake, and this may also be because the tunnel has a certain damping effect on this position. The T21 measuring point in the middle of the slope has obvious abrupt changes in the peak value of the marginal spectrum, and the characteristic frequency decreases. It shows that the seismic response of seismic wave at this location is obviously different from that of other measuring points under the action of low-intensity earthquake. The marginal spectral peak and characteristic frequency at the measuring point T20 decrease, and it shows that there is seismic damage at the position between relative elevation 0.75 and 0.875. With

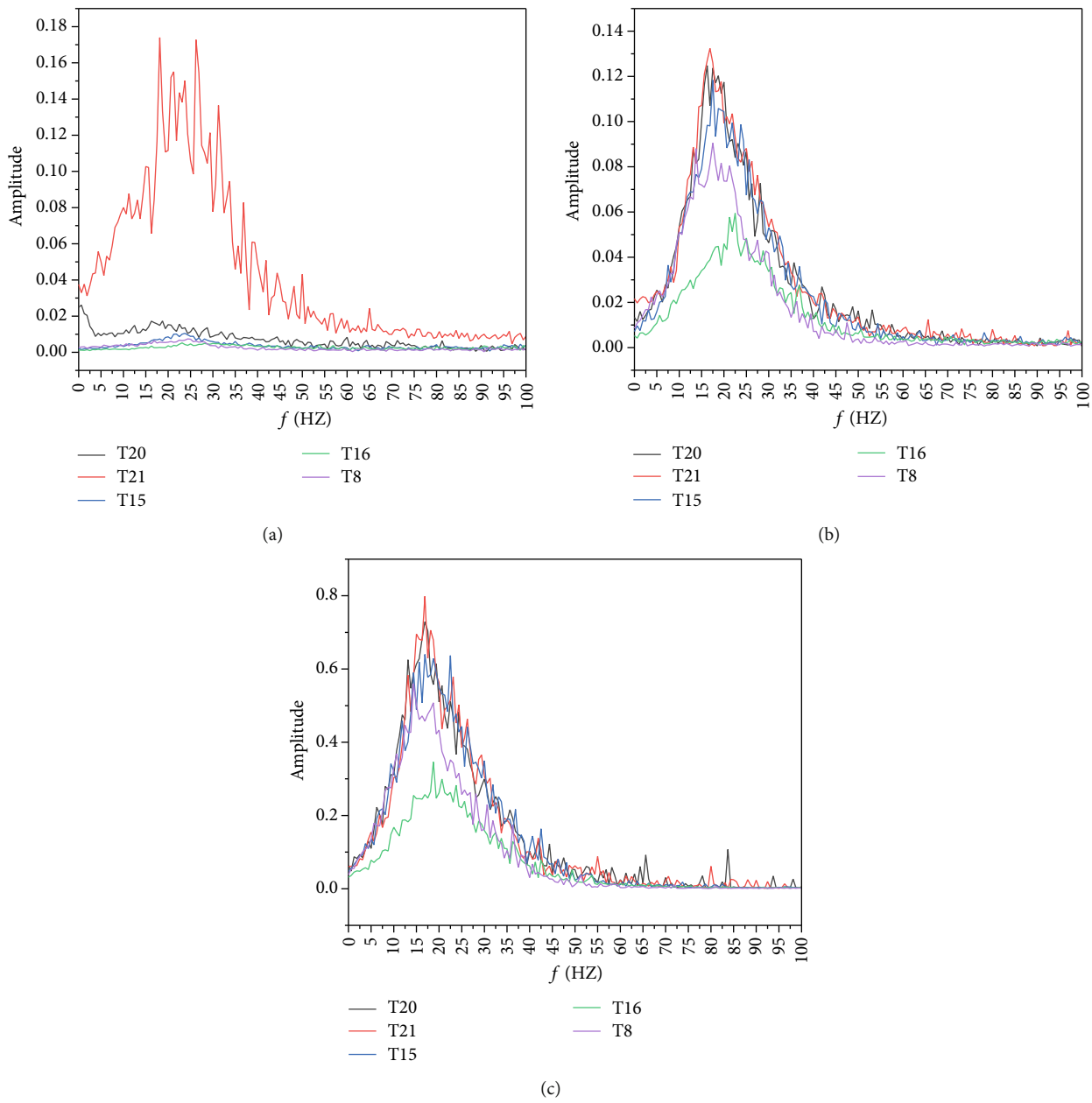

Figure 14: Marginal spectrum curve of each measuring point near the sliding surface under the action of earthquakes with different intensities. (a) Marginal spectrum curve of each measuring point under low-intensity earthquake. (b) Marginal spectrum curve of each measuring point under medium-intensity earthquake. (c) Marginal spectrum curve of each measuring point under high-intensity earthquake.

the increase of earthquake intensity (as shown in Figure 15(b)), the threshold reached by the damping effect of the tunnel. The peak value of the marginal spectrum of T16 measuring point at the middle and lower measuring points suddenly decreases, seismic energy cannot be completely transmitted in the wave body [33], and its characteristic frequency also mutated. This shows that the area between measuring point T8 (relative elevation 0.42) and measuring point T16 (relative elevation 0.5) has been damaged by earthquake under the action of medium-intensity earthquake (which can be effectively confirmed from the damage diagram in Figure 9(b). The marginal spectral peak and characteristic frequency at the measuring point T15 suddenly change, the middle slope is also further damaged under the action of medium-intensity earthquake, and the marginal spectral peak and characteristic frequency of the middle and upper slope are also slightly lower than those of the previous earthquake, which indicate that the seismic damage is also developing further. With the further increase of earthquake intensity (as shown in Figure 15(c)), its earthquake damage is similar to that of medium-intensity earthquake; however, the characteristic frequency of the middle

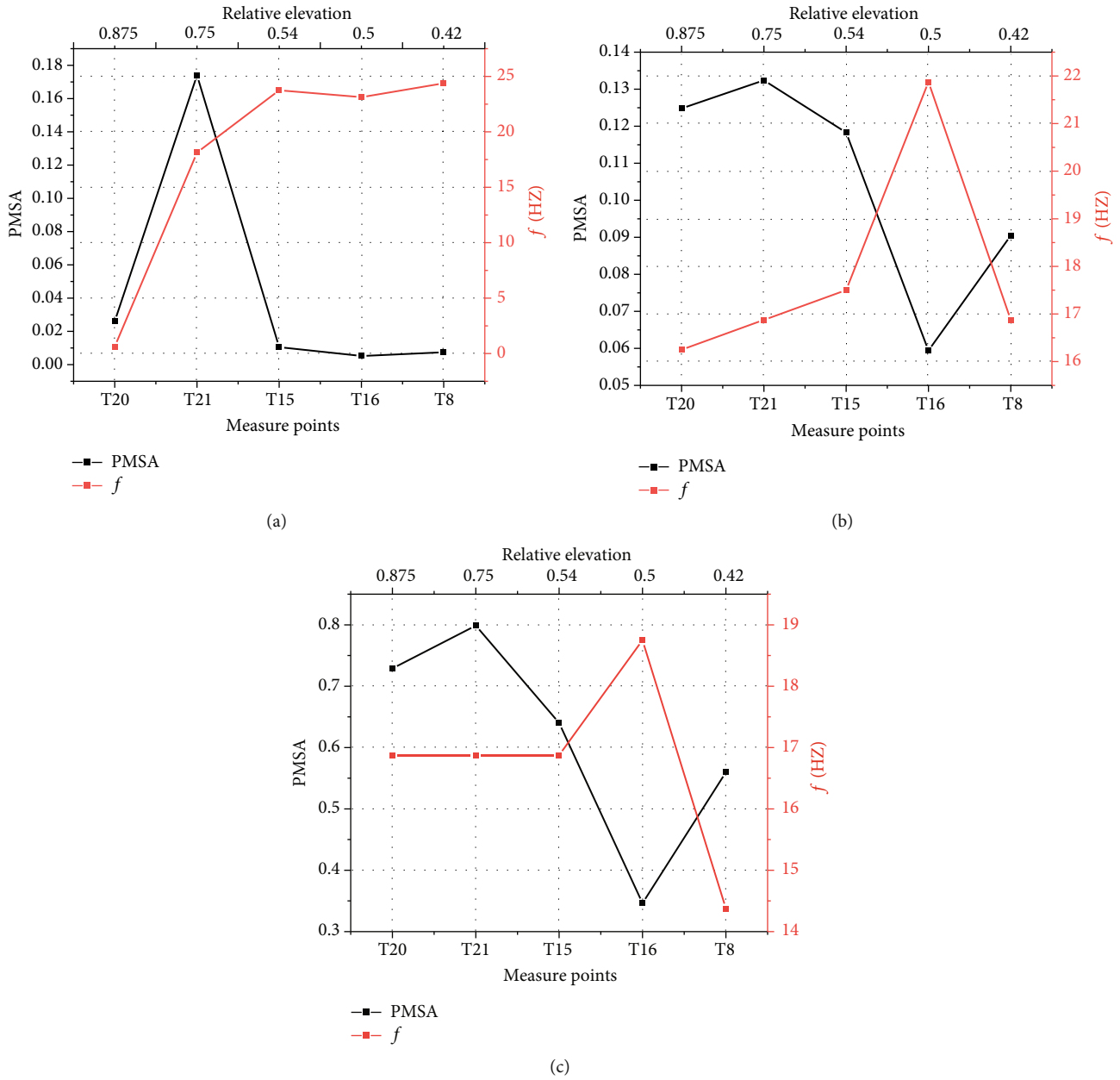

Figure 15: Marginal spectrum peak and characteristic frequency curve of each measuring point near the sliding surface under the action of earthquakes with different intensities. (a) Marginal spectrum peak and characteristic frequency curve of each measuring point under low-intensity earthquake. (b) Marginal spectrum peak and characteristic frequency curve of each measuring point under medium-intensity earthquake. (c) Marginal spectrum peak and characteristic frequency curve of each measuring point under high-intensity earthquake.

and upper slope (measuring points T15, T21, and T20) does not change, indicating that the middle and upper slope may have reached the critical limit of failure.

As can be seen from the above analysis, under the action of low-intensity earthquake, seismic damage occurs between the middle and upper parts of the slope (relative elevation 0.875~0.75), the seismic response of the middle slope (relative elevation 0.54~0.75) is different from that of other locations, and spalling blocks appear on the middle and upper slope. Under the action of moderate intensity earthquake, earthquake damage began to appear between the middle and lower slopes (relative elevation 0.42~0.5), the earthquake damage of the middle and upper slopes was further strengthened, the cracks in the middle and upper slope develop downward, the slope body tilts forward, and the spalling of the slope surface is enhanced. A large area of spalling occurs on the middle and lower slope, forming slope toe accumulation. Under the action of high-intensity earthquake, the seismic damage of the whole slope continues to increase, the middle and upper slope spall to form a depression, and the failure of the middle and lower slopes extends upward. A large amount of slope toe accumulation is formed at the slope toe.

Combined with the above analysis, the failure sequence of landslide with tunnel is as follows: failure of middle and upper slope→middle and lower slope fragmentation→the middle slope slides out; the failure mode can be summarized as extrusion and sliding out of the middle slope.

5. Conclusions and Recommendations

In order to study the dynamic characteristics of landslide with tunnel under horizontal seismic action and to provide reference for the reinforcement of landslide with tunnel, we carried out shaking table test of landslide-containing tunnel and extracted the acceleration response of the interface between landslide and slip zone and bedrock before and after tunnel. Through analysis of deformation characteristics, acceleration time-history curve, and spectrum characteristics of slope and correlation analysis of seismic response of various intensities, the results showed the following:

(1) Under the action of earthquakes of different intensity levels, the existence of tunnels has a certain effective damping effect on the upper landslide. In the landslide-containing tunnels, the upper slope is seriously damaged, and the lower slope foot is spalling and forming a large amount of accumulation at the slope foot, while the earthquake damage of the middle slope is always the least. Therefore, the middle and upper slope may be the weakest part of the landslide

(2) The tunnel and bedrock play a certain damping role in the transmission of low-intensity seismic waves, especially in the impact on the peak acceleration time of soil around the tunnel. The peak acceleration times in the bedrock in front of the tunnel are basically the same under the action of horizontal low-intensity seismic waves, but there is a big difference in the peak acceleration times under the coupling action of bedrock and tunnel after the local seismic waves pass through the tunnel. With the increase of earthquake intensity, the damping threshold of tunnel and bedrock reaches its limit, and the peak acceleration time is basically the same

(3) Under the coupling action of horizontal seismic wave with different peak value and tunnel, seismic wave will form complex seismic wave field. Under the coupling effect of tunnel and seismic wave, the acceleration amplification coefficient around the tunnel appears irregular distribution. At the interface between slip zone and slip body, the acceleration amplification coefficient of slope first decreases and then increases with elevation and basically remains unchanged when it reaches the angle position of slope 1/2 height. This indicates that the horizontal seismic action will be greatly affected in the position of stress concentration with tunnel landslide angle, and there should be effective damping structure in this position during the reinforcement of tunnel landslide

(4) There is a high correlation between seismic responses at all levels. When the preseismic response to the acceleration response of the landslide-containing tunnel is not considered, the acceleration response of the post-first-order seismic response to the slope and the structure will be lower than the real value. The continuous effect of fore shock response should be considered in seismic reinforcement of landslide-containing tunnel

(5) The sequence of failure of landslide mass containing tunnel is as follows: failure of middle and upper slope→middle and lower slope fragmentation→the middle slope slides out; the failure mode can be summarized as extrusion and sliding out of the middle slope

Data Availability

The data used to support the findings of this study are available from the corresponding author upon request.

Conflicts of Interest

The authors declare that they have no conflicts of interest.

Acknowledgments

The authors gratefully acknowledge the financial support by the National Key Research and Development Program of China (No. 2018YFC1504901), Science and Technology Program of Gansu Province (Nos. 21JR7RA738 and 21JR7RA739), Science and Technology Development Project of China Railway Research Institute Co., Ltd. (2017-KJ008-Z008-XB), Science and Technology Development Project of China Railway Ninth Bureau Group Co., Ltd. (No. DLF-ML-JSFW-2021-09), and Natural Science Foundation of Gansu Province (No. 145RJZA068).

References

[1] G. Urcioli and L. Picarelli, "Interaction between landslides and man-made works," *Proceedings of the Tenth International Symposium on Landslides and Engineered Slopes*, vol. 2, pp. 258–264, 2008.

[2] Y. Jiao, Z. Wang, X. Wang, A. C. Adoko, and Z. X. Yang, "Stability assessment of an ancient landslide crossed by two coal mine tunnels," *Engineering Geology*, vol. 159, no. 6, pp. 36–44, 2013.

[3] X. Wang, J. Lai, J. Qiu, W. Xu, L. Wang, and Y. Luo, "Geohazards, reflection and challenges in mountain tunnel construction of China: a data collection from 2002 to 2018," *Geomatics Natural Hazards and Risk*, vol. 11, no. 1, pp. 766–785, 2020.

[4] Z. Zhiguo, M. Mindong, Z. Qihua, and W. Zhongteng, "Research status and prospect of tunnel-landslide interaction and control protection technology," *Rock and Soil Mechanics*, vol. 42, no. 11, pp. 3101–3125, 2021.

[5] H. G. Wu, X. Y. Chen, and H. Ai, "Research on the deformation mechanism model test of tunnel-landslide parallel system," *Journal of Railway Engineering Society*, vol. 33, no. 11, 2016.

[6] H. G. Wu, X. Y. Chen, and H. Ai, "Research on the deformation mechanism model test of tunnel-landslide parallel system," *JOURNAL 0F RAILJWAY ENGINEERING SOCIETY*, vol. 33, no. 11, pp. 87–91+124, 2016.

[7] H. G. Wu, *Research on Deformation Mechanism and Control Technology of Tunnel-Landslide System*, China Academy of Railway Sciences, 2012.

[8] Z. P. Tao and D. P. Zhou, "The geological mechanics models of tunnel deformation at landslide site and engineering controlling measure," *JOURNAL 0F RAILJWAY ENGINEERING Society*, vol. 1, pp. 61–66, 2006.

[9] L. F. Pai and H. G. Wu, "Multi-attribute seismic data spectrum analysis of tunnel orthogonal underpass landslide shaking table test," *Soil Dynamics and Earthquake Engineering*, vol. 150, article 106889, 2021.

[10] M. He, L. R. Sousa, A. Müller et al., "Numerical and safety considerations about the Daguangbao landslide induced by the 2008 Wenchuan earthquake," *Journal of Rock Mechanics and Geotechnical Engineering*, vol. 11, no. 5, pp. 1019–1035, 2019.

[11] K. Konagai, S. Takatsu, T. Kanai, T. Fujita, T. Ikeda, and J. Johansson, "Kizawa tunnel cracked on 23 October 2004 Mid-Niigata earthquake: an example of earthquake-induced damage to tunnels in active-folding zones," *Soil Dynamics and Earthquake Engineering*, vol. 29, no. 2, pp. 394–403, 2009.

[12] C. C. Lu and J. Hwang, "Nonlinear collapse simulation of Daikai subway in the 1995 Kobe earthquake: necessity of dynamic analysis for a shallow tunnel," *Tunnelling and Underground Space Technology*, vol. 87, pp. 78–90, 2019.

[13] X. P. Zhang, Y. J. Jiang, and M. Kazuhiko, "Mountain tunnel under earthquake force: a review of possible causes of damages and restoration methods," *Journal of Rock Mechanics and Geotechnical Engineering*, vol. 12, no. 2, pp. 414–426, 2020.

[14] Y. M. Wen, C. L. Xin, Y. S. Shen, Z. M. Huang, and B. Gao, "The seismic response mechanisms of segmental lining structures applied in fault-crossing mountain tunnel: the numerical investigation and experimental validation," *Soil Dynamics and Earthquake Engineering*, vol. 151, article 107001, 2021.

[15] L. F. Pai, H. G. Wu, and H. M. Ma, "Seismic optimization of soil slope reinforced by multi-anchor point piles under earthquake by shaking table test," *Chinese Journal of Rock Mechanics and Engineering*, vol. 40, no. 4, pp. 751–765, 2021.

[16] W. Y. Sun, S. H. Yan, Q. G. Ma et al., "Dynamic response characteristics and failure mode of a bias loess tunnel using a shaking table model test," *Transportation Geotechnics*, vol. 31, article 100659, 2021.

[17] X. L. Jiang, J. Q. Zhang, Y. Hui, F. F. Zhao, and W. C. Fan, "Seismic dynamic response characteristics of slope of double-arch tunnel under multivariate factors," *Journal of vVibration Engineering*, vol. 33, no. 6, pp. 1291–1301, 2020.

[18] J. Q. Zhang, X. L. Jiang, H. Yang, F. F. Zhao, X. Liu, and H. T. Shi, "Study on seismic response characteristics of slope with double-arch tunnel," *Chinese Journal of Applied Mechanics*, vol. 38, no. 2, pp. 597–606, 2021.

[19] M. Ramu, V. P. Raja, and P. R. Thyla, "Establishment of structural similitude for elastic models and validation of scaling laws," *KSCE Journal of Civil Engineering*, vol. 17, no. 1, pp. 139–144, 2013.

[20] J. Ayres, R. Moura, P. Santos, and M. Terezinha, "Exploring similarity relations according to different contexts in mining generalized association rules," *International Conference on Enterprise Information Systems*, vol. 141, pp. 137–152, 2013.

[21] C. L. Zhang, G. Jiang, L. Su, D. Lei, W. Liu, and Z. Wang, "Large-scale shaking table model test on seismic performance of bridge-pile-foundation slope with anti-sliding piles: a case study," *Bulletin of Engineering Geology and the Environment*, vol. 79, no. 3, pp. 1429–1447, 2020.

[22] H. Dou and P. M. Byrne, "Model studies of boundary effect on dynamic soil response," *Canadian Geotechnical Journal*, vol. 34, no. 3, pp. 460–465, 1997.

[23] K. F. Al-Raheem, A. Roy, K. P. Ramachandran, D. K. Harrison, and G. Steven, "Rolling element bearing faults diagnosis based on autocorrelation of optimized: wavelet de-noising technique," *International Journal of Advanced Manufacturing Technology*, vol. 40, no. 3-4, pp. 393–402, 2009.

[24] B. T. Li, W. G. Qiu, X. G. Qi, Z. H. Deng, and H. Hu, "Experimental study on seismic response of longitudinal cracked tunnel lining with shaking table," *Journal of Southwest Jiaotong University*, vol. 56, no. 1, pp. 20–27+55, 2021.

[25] Chongqing transportation research and design Institute, *JTG 3370.1-2018 Highway Tunnel Design Specification*, People's Communications Press, Beijing, 2018, China (in chinese).

[26] China Railway First Highway Survey and Design Research Institute Co., *Ltd.Jtg C20-2016 Highway Engineering Geological Survey Code*, People's Communications Press, Beijing, 2011, China (in chinese).

[27] J. T. Liu, *Large-Scale Model Test Study of Pipeline Crossing Landslide Interaction*, Chengdu University of Technology, 2012, in chinese.

[28] T. Ikuo, "Seismic wave propagation in elastic soil with continuous variation of shear modulus in the vertical direction," *Soils and Foundations*, vol. 36, no. 1, pp. 61–72, 1996.

[29] Y. Changwei, Z. Liang, D. Longjun et al., "Research on the difference of dynamic responses between bedding and toppling rock slopes based on shaking table test," *Chinese Journal of Rock Mechanics and Engineering*, vol. 41, no. 2, pp. 271–281, 2022.

[30] D. Q. Song, X. L. Liu, J. Huang, and J. M. Zhang, "Energy-based analysis of seismic failure mechanism of a rock slope with discontinuities using Hilbert-Huang transform and marginal spectrum in the time-frequency domain," *Landslides*, vol. 18, pp. 105–123, 2021.

[31] N. E. Huang, Z. Shen, S. R. Long et al., "The empirical mode decomposition and the Hilbert spectrum for nonlinear and non-stationary time series analysis," *Proceedings of the Royal Society of London. Series A: mathematical, physical and engineering sciences*, vol. 454, no. 1971, pp. 903–995, 1998.

[32] N. E. Huang, Z. Shen, and S. R. Long, "A new view of nonlinear water waves: the Hilbert spectrum," *Annual Review of Fluid Mechanics*, vol. 31, no. 1, pp. 417–457, 1999.

[33] G. Fan, J. J. Zhang, and J. W. Zhou, *Seismic Response and Stability Time-Frequency Analysis Method of Layered Rock Slope*, Southwest Jiaotong University Press, Sichuan: China, 2020, in Chinese.

[34] Y. F. Yu, *Strength Characteristics and Seismic Failure Mode of Loess Slope with Structural Joints*, Lanzhou Institute of Seismology, China Earthquake Administration, 2020.

[35] X. Yang, *Failure Mode and Dynamic Response of the Bedrock and Overburden Layer Slope*, Southwest Jiaotong University, 2019.

[36] R. M. Wang, *Experimental Study on Dynamic Response and Failure Mode of Different Soil Slopes under Earthquake*, Southwest Jiaotong University, 2016.